Eur. Phys. J. B **50**, 521–526 (2006)
DOI: 10.1140/epjb/e2006-00179-8

THE EUROPEAN PHYSICAL JOURNAL B

Theoretical calculations of the high-pressure phases of ZnF_2 and CdF_2

X. Wu and Z. Wu[a]

Beijing Synchrotron Radiation Facility, Institute of High Energy Physics, Chinese Academy of Sciences, Beijing 100049, P.R. China

Received 27 November 2005
Published online 17 May 2006 –

Abstract. First-principles calculations based on density functional theory were used to study the high-pressure phases of both ZnF_2 and CdF_2. We found that the sequence of the pressure-induced phase transitions is: Rutile ($P4_2/mnm$) → $CaCl_2$($Pnnm$) → PdF_2 (Pa-3) and CaF_2 ($Fm3m$) → $PbCl_2$ ($Pnma$) → Ni_2In ($P6_3/mmc$) for ZnF_2 and CdF_2 respectively. In ZnF_2 the behavior of the ground-state total energy, of the Gibbs free energy and of the lattice constant vs. pressure shown that the phase transition at 4 GPa from the rutile-type phase to the $CaCl_2$-type phase is a second-order phase transition. The mechanism of the structural change was also revealed by the transition from the $PbCl_2$-type phase to the Ni_2In-type phase in CdF_2. Moreover, the high-pressure behavior of divalent metal fluorides was compared and discussed.

PACS. 61.50.Ks Crystallographic aspects of phase transformations; pressure effects – 71.15.-m Methods of electronic structure calculations

1 Introduction

The fluorides with divalent metals e.g. AF_2 compounds (A = Ca, Sr, Ba, Pb, Mg, Mn, Zn, Cd etc.) are systems with a great theoretical and experimental interests [1–12] because of their properties and applications in different fields. As an example, due to its excellent transmission properties over a wide wavelength range from the UV to IR domain, CaF_2 is a system commonly used as a lens material for photolithographic applications at wavelengths in the deep ultraviolet region. Similarly, PbF_2 is an important scintillating material that exhibits also a superionic conductivity behavior [13,14] while ZnF_2 exhibits a large anisotropy of its dielectric properties when doped with lithium [15]. Always with doping, CdF_2 may be converted into a semiconducting material using the elements of the III column of the periodic table [16]. In all these cases the unique physical properties are correlated to the crystal structure of these AF_2 systems, that at ambient condition it may be divided into two groups: the rutile-type ($P4_2/mnm$) and the fluorite-type ($Fm3m$). At higher pressure, AF_2 compounds undergo to a series of phase transitions that affect their physical properties [7,12]. For the rutile-type (MgF_2 [5,17]), the sequence of pressure-induced phase transition is the following:

Rutile ($P4_2/mnm$) → $CaCl_2$ ($Pnnm$) → PdF_2 (Pa-3)

while for the fluorite-type is

CaF_2 ($Fm3m$) → $PbCl_2$ ($Pnma$) → Ni_2In ($P6_3/mmc$)

fulfilled by CaF_2 [7,12], BaF_2 [3,18,19] and PbF_2 [4]). Actually, pressure is really a critical parameter for structural stabilities, electronic and optical properties of AF_2 systems.

ZnF_2 and CdF_2 are important optical materials that have been investigated mainly looking at the effects induced by doping on the optical properties. Recently the high-pressure structural behavior of ZnF_2 has been investigated by Raman spectroscopy up to 6.8 GPa, showing that a phase transition from the rutile-type to the $CaCl_2$-type structure occurs at a pressure of about 4.5 GPa [11]. As far as we know, no high-pressure structural data are available for both ZnF_2 and CdF_2. Therefore in this manuscript we investigated by means of electronic structure calculations the high-pressure phases of both ZnF_2 and CdF_2. The method has been proven to be successful in previous phase transition investigations [12,20]. Moreover, we will further discuss the general high-pressure behavior of the divalent metal fluoride system.

2 Calculation method

While at ambient conditions ZnF_2 is a rutile-type difluoride and its possible high-pressure phases are: $P4_2/mnm$, $Pnnm$ and Pa-3 according to experimental data [11] and the results of its analogue material MgF_2 [5,17], CdF_2

[a] e-mail: wuzy@ihep.ac.cn

is a fluorite-type structure and its candidate phases are $Fm3m$, $Pnma$, and $P6_3/mmc$. To start the analysis in these systems we select the experimental unit cell parameters or the analogue materials.

The first-principle calculations performed in this manuscript are based on the density functional theory (DFT). The total energies have been calculated within the full potential augmented plane wave (FPAPW) plus the local orbitals (lo) method, implemented in the WINE2K code [21]. The effects of the approximation to the exchange-correlation energy were treated by the generalized gradient approximation (GGA) [22]. In order to increase the reliability and to obtain a reasonable comparison, we used the same radius of the muffin-tin sphere for the same kind of atom in all calculations. The muffin-tin radii of Zn, Cd and F were chosen 1.6, 1.7 and 1.8 a.u. respectively. In the LAPW calculations, we set the energy threshold between core and valence states at –7.0 Ry for the ZnF_2 and –8.0 Ry for the CdF_2. For the number of the plane waves, the criterion selected was the muffin-tin radius multiplied by K_{max}. We set $R_{MT}K_{max}$ equal to 7.0 The K integration over the Brillouin zone was specified to be 1000 k-points. For each crystalline phase, we calculated the minimum total energy of the unit cell for a number of different volumes. The structure optimization of the $Fm3m$ phase was not performed but we specified the convergence criterion (the different charge <0.0001) in the self-consistency cycle. In the case of the $Pnnm$, $Pnma$ and $P4_2/mnm$ phases, we optimized the b/a ratio and (or) the c/a ratio for each volume and relaxed all the independent internal atomic coordinates until the forces on every atom were below the value of 1 mRy/bohr. For the $P6_3/mmc$ phase, the c/a ratio was also optimized and the convergence criterion was chosen the same of the $Fm3m$ phase.

Once the minimum total energies of every phase was obtained at each volume, we fit data with the Murnaghan equation of state [23]:

$$E(V) = E_0 - \frac{B_0 V_0}{B_0' - 1} + \frac{B_0 V}{B_0'}\left[\frac{(V_0/V)^{B_0'}}{B_0' - 1} + 1\right] \quad (1)$$

where B_0 and B_0' are the bulk modulus and its derivative, E_0 is the ground-state total energy and V_0 is the equilibrium volume. However, the relevant thermodynamic potential is the Gibbs free energy (G) and the most stable structure is that with the lowest G. This study refer to the temperature $T = 0$ K so that G is

$$G(P) = E_0 + \frac{B_0 V_0}{B_0' - 1}\left[\left(1 + \frac{B_0'}{B_0}P\right)^{\frac{B_0'-1}{B_0'}} - 1\right]. \quad (2)$$

If the transition between two phases occurs, at the transition pressure P_T, G is the same for both phases. As a consequence, the transition pressure may be obtained as the negative slope of the common tangent between the $E_{tot}(V)$ curves of the two phases.

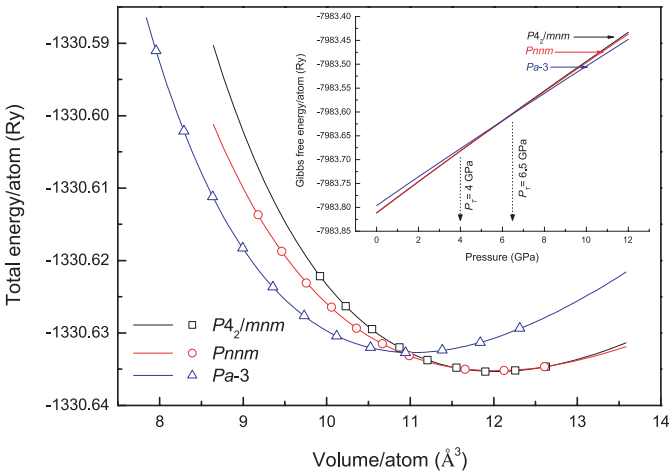

(A) ZnF_2

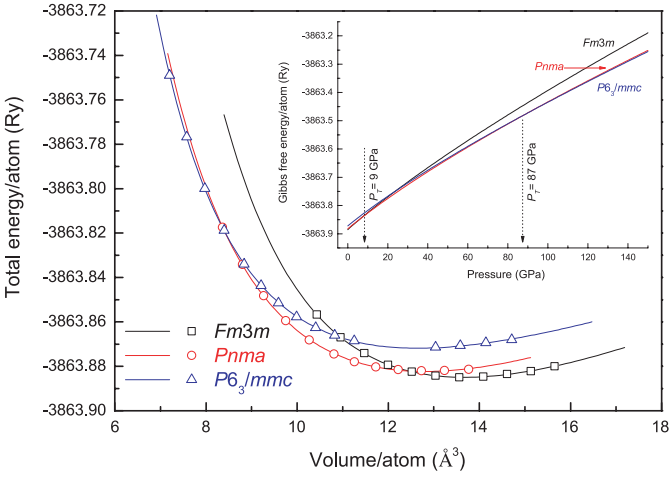

(B) CdF_2

Fig. 1. Calculations of the ground-state total energy vs. volume for the three candidate phases for the two systems: ZnF_2(A), CdF_2(B). In the inset the calculated Gibbs free energy vs. pressure for the corresponding phases: ZnF_2 (A), CdF_2 (B).

3 Results and discussion

The ground-state total energy as a function of the volume for ZnF_2 and CdF_2, in each of candidate high-pressure phases, is given in Figure 1. The solid lines are the fit of the calculation data using the Murnaghan equation of state [Eq. (1)]. The theoretical ground-state parameters (lattice constants and B_0) are listed in Table 1 and compared with the available experimental data [1,24,25]. The GGA calculations overestimate the lattice constants by 2% while the bulk modulus of rutile-type ZnF_2 is in good agreement with experiments. However, these values are satisfactory and within the typical precision of GGA-DFT calculations.

Figure 1a shows the phase transition sequence of ZnF_2, e.g. $P4_2/mnm \rightarrow Pnnm \rightarrow Pa$-3. The first transition

Table 1. Comparison of calculated (this work) and experimental values of the lattice constant and the bulk modulus of ZnF_2 and CdF_2.

	ZnF_2				CdF_2			
	$P4_2/mnm$		$Pnnm$	Pa-3	$Fm3m$		$Pnma$	$P6_3/mmc$
	theory	experiment	theory	theory	theory	experiment	theory	theory
Lattice parameter (Å)	$a = 4.7534$ $c = 3.1943$	$a = 4.7038$ $c = 3.1336$ [24]	$a = 4.7872$ $b = 4.7451$ $c = 3.1734$	$a = 5.0594$	$a = 5.4739$	$a = 5.3885$ [25]	$a = 5.9270$ $b = 3.6746$ $c = 7.0543$	$a = 3.7602$ $c = 6.1965$
Bulk modulus (GPa)	107	103.8 [1]	87	116	96	–	85	71

Table 2. Comparison of calculation and experimental data of the transition pressure and volume collapse of the phase transition boundaries for ZnF_2 and CdF_2.

	ZnF_2			CdF_2	
	$P4_2/mnm$-to-$Pnnm$		$Pnnm$-to-Pa-3	$Fm3m$-to-$Pnma$	$Pnma$-to-$P6_3/mmc$
	theory	experiment	theory	theory	theory
Transition pressure (GPa)	4	4.5 [11]	6.5	9	87
Volume collapse (%)	0.6	–	6.4	6.7	2.1

($P4_2/mnm$ to $Pnnm$) takes place at 4 GPa and the second ($Pnnm$ to Pa-3) at 6.5 GPa according to the Gibbs free energy as a function of pressure, as shown in the inset of Figure 1a. The phase transition critical pressure (4 GPa) obtained by our calculation is consistent with Raman experiments (4.5 GPa) by Perakis et al. [11]. In Figure 1b we shows that the sequence of the CdF_2 system: $Fm3m \rightarrow Pnma \rightarrow P6_3/mmc$ with transition pressures of 9 GPa and 87 GPa respectively. The volume collapses at the phase transition boundaries for both ZnF_2 and CdF_2 have been calculated at the related transition pressures as reported in Table 2 for these systems.

The Landau theory predicts a second-order ferroelastic phase transition from the rutile-type phase to the $CaCl_2$-type that should involve a softening of the Raman-active B_{1g} mode [26,27], such as in the rutile-type oxides GeO_2 [28] and SnO_2 [29]. However, in the rutile-type ZnF_2 the B_{1g} mode has not been observed yet in high-pressure Raman experiment performed with a diamond anvil cell (DAC) probably because of its weak intensity [11]. In the present work, the $E - V$ curves of the rutile and $CaCl_2$ phases overlap in the average percent atom volume between 11.1 and 13.2 Å^3, as shown in Figure 1a. A behavior typical of a second-order phase transition. At the same time, no discontinuities in both cell constants and volume are observed, e.g. the volume change is only 0.6% at the critical pressure (4.0 GPa) suggesting that the $P4_2/mnm$-to-$Pnnm$ transition is a second-order phase transition. While according to the behaviors of the $E - V$ curves the phase transition from the $CaCl_2$-type structure to the PdF_2-type is clearly of the first-order, the $G - P$ curves and the volume collapse at the critical pressure of 6.5 GPa. The structures of the rutile-type, the $CaCl_2$ and the PdF_2 phases are shown in Figure 2. The optimized lattice parameters shown that the oxygen x-coordinate of the rutile-type phase decreases as a function of pressure, indicating that the two apical Zn-F distances lying in the ab plane decrease much more than the four equatorial distances. As a consequence, the oxygen ions are not longer in the [110] and [1–10] planes in a $CaCl_2$-type structure (see Fig. 2b). With an additional compression, the coordination number of Zn increases from 6 ($CaCl_2$-type) to 6 + 2 (the PdF_2-type) with a large increase of the density. Actually, the high-pressure structural behavior of ZnF_2 looks very similar to that of rutile-type dioxides and halides, such as SnO_2 [29], GeO_2 [28,30], ZrO_2 [31] and MgF_2 [5,17].

In the case of CdF_2, the coordination number of Cd increases from 8 (fluorite-type) to 9 ($PbCl_2$-type), then to 11 (Ni_2In-type) so that the Cd^{2+} ionic radius increases with pressure. In order to understand the mechanism of structural change from the $PbCl_2$-type phase to the Ni_2In-type phase, we may describe the hexagonal Ni_2In structure as an orthorhombic structure, with a space group $Pnma$, where $a_0 = c_h$, $b_0 = a_h$, $c_0 = 3^{1/2}a_h$, the Cd atomic positions are (1/4, 1/4, 1/12) and those of F are (1/4, 1/4, 5/12) and (0,3/4,1/4) [3]. Projection along the b axis of these two orthorhombic structures is shown in Figure 3. According to the optimized atomic coordinates of the $Pnma$ phase at various pressures, the positions of some F ions shifts are labeled with arrows in Figure 3. Looking at Figure 3 the ∠F5-F3-F6 increases with pressure in the $PbCl_2$ structure and become 180° in the Ni_2In structure. The F1 ion shifts to the coordination polyhedron of Cd1 under compression, and finally becomes a coordination of Cd1 in the $P6_3/mmc$ due to the F1-Cd1 bond distance decreasing suddenly. The other F^{1-} ion in the background has the same behavior, so that the coordination numbers of Cd^{2+} increase by two to become eleven at the phase transition from $Pnma$ to $P6_3/mmc$. In other words, this phase transition induces a rotation of the coordination of the Cd polyhedra along the b axis. Similar behaviors have been observed in CaF_2 [12], BaF_2 [3,18,19] and PbF_2 [4].

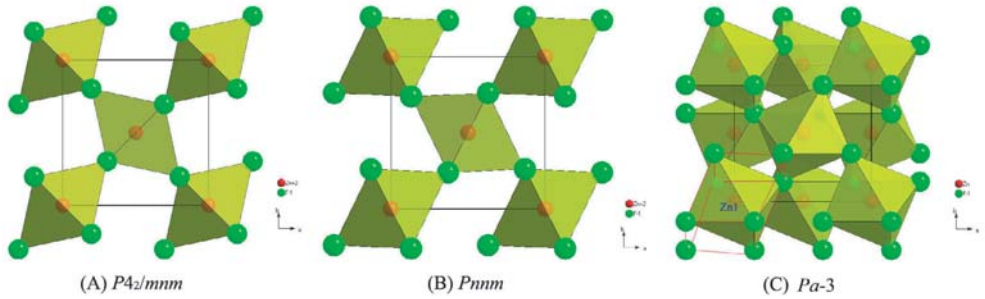

Fig. 2. The crystal structures of the ZnF_2 compound with different space groups: $P4_2/mnm$(a), $Pnnm$ (b) and Pa-3 (c). The 6 + 2 coordination polyhedron of the Pa-3-type phase is outlined by red lines in the right C panel.

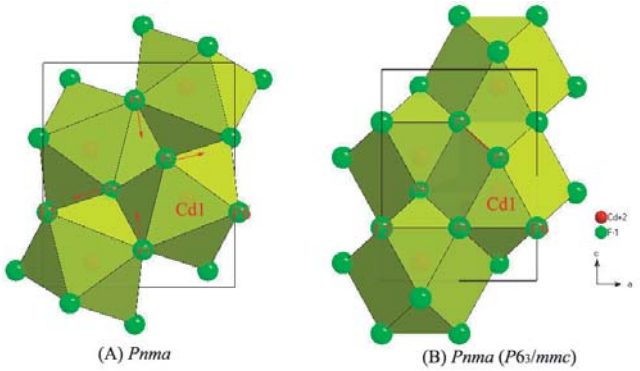

Fig. 3. Projection along the b axis of the two orthorhombic phases of the CdF_2. (a) $PbC1_2$-type structure; (b) Ni_2In-type structure.

The GGA electron energy band structures of both ZnF_2 and CdF_2 have been calculated increasing pressure. The influence of the pressure on the electronic structure is summarized looking at the behavior of the energy gap in Figure 4. The band gap of ZnF_2 is direct from Γ^V to Γ^C, and it increases with pressure. On the contrary, in the CdF_2 is indirect ($W^V \rightarrow \Gamma^C$) in the $Fm3m$ phase, becomes direct ($\Gamma^V \rightarrow \Gamma^C$) in the $Pnma$ phase and finally again indirect ($K^V \rightarrow \Gamma^C$) in the $P6_3/mmc$ phase. Also the gap of CdF_2 increases with pressure, but undergoes a sudden decrease at the phase transition from the $Pnma$ to the $P6_3/mmc$ (Fig. 4b). The solid lines in Figure 4 are the least-square fit of the calculated data using a nonlinear pressure-dependent function:

$$E(P) = E(0) + \alpha P + \beta P^2$$

where energy E is in eV, pressure P is in GPa and α and β are the band gap pressure coefficients. In Table 3 the band gap pressure coefficients of both ZnF_2 and CdF_2 are listed.

The high-pressure behavior of AF_2 (A = Ni, Mg, Zn, Co, Mn, Cd, Ca, Pb and Ba) is summarized in Figure 5. For the rutile-type, the sequence of pressure-induced phase transition is Rutile $\rightarrow$ $CaCl_2$ $\rightarrow$ PdF_2, while CaF_2 $\rightarrow$ $PbCl_2$ $\rightarrow$ Ni_2In is for the fluorite-type. The bulk modulus decreases with the radius of the metal ion increasing for the same structure, as shown in Figure 5. The

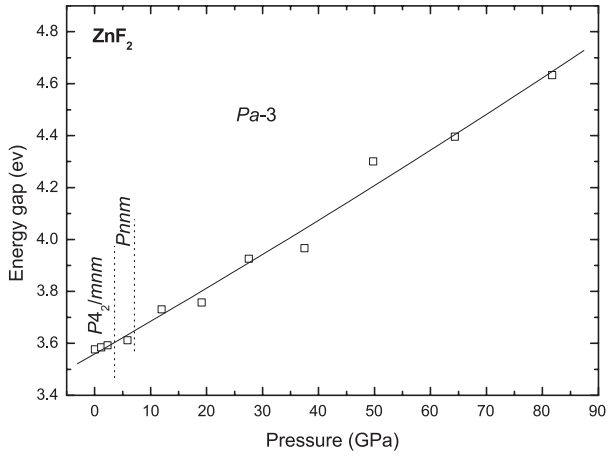

(a)

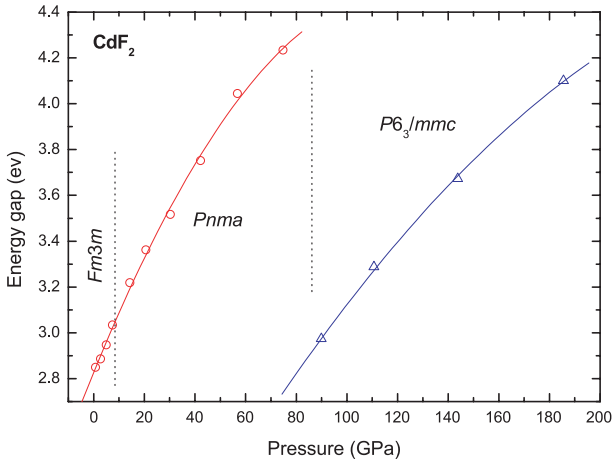

(b)

Fig. 4. The energy band gap of ZnF_2 (a) and CdF_2 (b) vs. pressure.

bulk modulus decreases in the high-pressure phase for the fluorite-type systems as a downward arrow $\downarrow$ indicates in Figure 4, but that of BaF_2 increases as an upward arrow $\uparrow$ shows. The reason for this discrepancy is not clear, and it is necessary to be analyzed in later work. For the rutile-type systems, the bulk modulus decreases firstly,

Table 3. Pressure coefficients for the energy band gaps of ZnF_2 and CdF_2.

	ZnF_2	CdF_2	
	$P4_2/mnm$, $Pnnm$ and Pa-3	$Fm3m$ and $Pnma$	$P6_3/mmc$
α (eV/GPa)	1.243×10^{-2}	2.712×10^{-2}	2.131×10^{-2}
β (eV/GPa^2)	1.082×10^{-5}	-1.097×10^{-4}	-3.474×10^{-4}

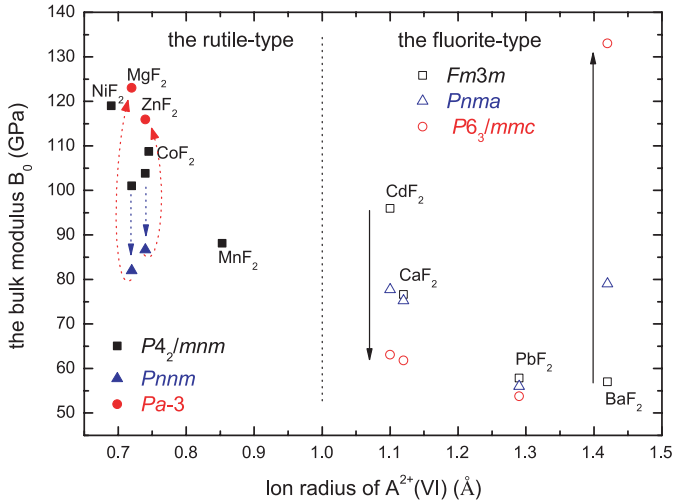

Fig. 5. Correlation plot between the radius of divalent metal ions and bulk modulus (B_0). Experimental data for MnF_2, CoF_2 and NiF_2 are from reference [1], BaF_2 [3], PbF_2 [4], MgF_2 [5], CaF_2 [12], ZnF_2 and CdF_2 are from the present work.

and then increases as the arrows show in the left of Figure 5.

In present analysis we did not consider the post-PdF_2 phase in ZnF_2, however experimental and theoretical data assigned it to the cotunnite-type (α-$PbCl_2$) structure, such as MgF_2 [5] and SiO_2 [32]. In CdF_2, CaF_2 and BaF_2 the $PbCl_2$-type phases will continuously transform into the Ni_2In-type at higher pressures. However, data of Haines et al. do not support the suggested trend towards the Ni_2In-type structure for the $PbCl_2$-type MgF_2 and the phase appears stable at least up to 227 GPa [5]. Similarly, $PbCl_2$-type metal dioxides such as PbO_2 [33] and ZrO_2 [31] do not show a trend towards a phase transition. Therefore, the high-pressure phase transitions appear to be driven mainly by the cation to anion radius ratio [3,30]. From our data we may extrapolate that the PdF_2-type ZnF_2 system should transform into a $PbCl_2$ phase at higher pressure, due to the similar radius between Mg and Zn ions, e.g., the radius of the $^{VI}Mg^{2+}$ is 0.72 Å and that of $^{VI}Zn^{2+}$ is 0.74 Å [34].

4 Conclusion

We presented here ab initio calculations of a series of high-pressure phases of ZnF_2 and CdF_2. The ZnF_2 system undergoes first to a phase transition at 4 GPa from the rutile-type structure ($P4_2/mnm$) to the $CaCl_2$-type structure ($Pnnm$), in good agreement with Raman experimental results, then at 6.5 GPa the system transforms into a PdF_2-type (Pa-3) structure. Our data, suggest that ZnF_2 will further transform into a $PbCl_2$-type structure at higher pressure. The behavior of the ground-state total energies, the Gibbs free energies and the lattice constants vs. pressure suggest that the $P4_2/mnm$-to-$Pnnm$ is a second-order phase transition. The CdF_2 system with a fluorite-type structure transforms into a $PbCl_2$-type structure at 9.0 GPa, then into a Ni_2In-type structure at 87 GPa. The $PbCl_2$-to-Ni_2In phase transition is associated to a rotation of the Cd coordination polyhedra along the b axis. Moreover, data showed that the energy band gaps of ZnF_2 and CdF_2 increase with pressure, except in the case of CdF_2 at the phase transition boundary from the $Pnma$ to the $P6_3/mmc$ structure. Finally, from the observed behaviors we may claim that the high-pressure behavior of all divalent metal fluorides indicate that both bulk modulus and the critical pressure decrease when the metal ion radius increases.

Z.Y. Wu acknowledges the financial support of the Outstanding Youth Fund (10125523), the Key Important Nano-Research Project (90206032) of the National Natural Science Foundation of China and the Pilot Project of the Knowledge Innovation Program of the Chinese Academy of Sciences (KJCX2-SW-N11). Thanks are due to A. Marcelli for many helpful discussions and criticisms.

References

1. D. Gerlich, S. Hart, D. Whittal, Phys. Rev. B **29**, 2142 (1984)
2. L. Gerward, J.S. Olsen, S. Steenstrup, S. Åsbrink, A. Waskowska, J. Appl. Cryst. **25**, 578 (1992)
3. J.M. Léger, J. Haines, A. Atouf, O. Schulte, S. Hull, Phys. Rev. B **52**, 13247 (1995)
4. A. Costales, M.A. Blanco, R. Pandey, J.M. Recio, Phys. Rev. B **61**, 11359 (2000)
5. J. Haines, J.M. Léger, F. Gorelli, D.D. Klug, J.S. Tse, Z.Q. Li, Phys. Rev. B **64**, 134110 (2001)
6. S. Speziale, T.S. Duffy, Phys. Chem. Minerals **29**, 465 (2002)
7. V. Kanchana, G. Vaitheeswaran, M. Rajagopalan, Phys. B **328**, 283 (2003)
8. M. Verstraete, X. Gonze, Phys. Rev. B **68**, 195123 (2003)
9. R. Khenata, B. Daoudi, M. Sahnoun, H. Baltache, M. Rérat, A.H. Reshak, B. Bouhafs, H. Abid, M. Driz, Eur. Phys. J. B **47**, 63 (2005)

10. F.S. El'kin, O.B. Tsiok, L.G. Khvostantsev, V.V. Brazhkin, J. Exp. Theoret. Phys. **100**, 971 (2005)
11. A. Perakis, D. Lampakis, Y.C. Boulmetis, C. Raptis, Phys. Rev. B **72**, 144108 (2005)
12. X. Wu, S. Qin, Z.Y. Wu, Phys. Rev. B **73**, in press
13. G.A. Samara, J. Phys. Chem. Solids **40**, 509 (1979)
14. S.E. Derenzo, W.W. Moses, J.L. Cahoon, R.C.C. Perera, J.E. Litton, IEEE Trans. Nucl. Sci. **37**, 203 (1990)
15. T. Roth, J. Appl. Phys. **44**, 1056 (1973)
16. A.I. Ritus, A.V. Pronin, A.A. Volkov, P. Lunkenheimer, A. Loidl, A.S. Shcheulin, A.I. Ryskin, Phys. Rev. B **65**, 5209 (2002)
17. V. Kanchana, G. Vaitheeswaran, M. Rajagopalan, J. Alloys and Compounds **352**, 60 (2003)
18. V. Kanchana, G. Vaitheeswaran, M. Rajagopalan, J. Alloys and Compounds **359**, 66 (2003)
19. H. Jiang, R. Pandey, C. Darrigan, M. Rérat, J. Phys.: Condens. Matter **15**, 709 (2003)
20. X. Wu, Y.H. Dong, S. Qin, M.I. Abbas, Z.Y. Wu, Solid State Communication **136**, 416 (2005)
21. P. Blaha, K. Schwarz, WIEN2k, Vienna University of Technology Austria (2002)
22. J.P. Perdew, K. Burke, M. Ernzerhof, Phys. Rev. Lett. **77**, 3865 (1996)
23. F.D. Murnaghan, Proc. Natl. Acad. Sci. USA **50**, 667 (1944)
24. N.J. O'Toole, V.A. Streltsov, Acta Cryst. B **57**, 128 (2001)
25. H.M. Haendler, W.J. Bernard, J. Am. Chem. Soc. **73**, 5218 (1951)
26. E.K.H. Salje, *Phase transitions in ferroelastic and co-elastic crystals* (Cambridge University Press, Cambridge, 1990)
27. H.T. Stokes, D.M. Hatch, *Isotropy subgroups of the 230 crystallographic space groups* (World Scientific, Singapore, 1988)
28. J. Haines, J.M. Léger, C. Chateau, R. Bini, L. Ulivi, Phys. Rev. B **58**, R2909 (1998)
29. H. Hellwig, A.F. Goncharov, E. Gregoryanz, H.K. Mao, R.J. Hemley, Phys. Rev. B **67**, 174110 (2003)
30. J. Haines, J.M. Léger, C. Chateau, A.S. Pereira, Phys. Chem. Minerals **27**, 575 (2000)
31. J.K. Dewhurst, J.E. Lowther, Phys. Rev. B **57**, 741 (1998)
32. A.R. Oganov, M.J. Gillan, G.D. Price, Phys. Rev. B **71**, 064104 (2005)
33. J. Haines, J.M. Léger, O. Schulte, J. Phys.: Condens. Matter **8**, 1631 (1996)
34. R.D. Shannon, Acta Cryst. A **32**, 751 (1976)